AC

KUNS-1489 / January, 1998

Scattering Observables of the NN and YN Interactions In the SU_6 Quark Model

T. Fujita, Y. Fujiwara, and C. Nakamoto*

Department of Physics, Kyoto University, Kyoto 606-01

Y. Suzuki

Department of Physics, Niigata University, Niigata 950-21

Abstract

Scattering observables of the NN and YN interactions are investigated in a recent quark model developed for a simultaneous description of the NN and YN systems. The model is formulated in the $(3q)$-$(3q)$ resonating-group method, and incorporates a phenomenological quark-confining potential, the full Fermi-Breit interaction with explicit quark-mass dependence, and minimum effective meson-exchange potentials of scalar and pseudo-scalar meson nonets directly coupled to quarks. Characteristic features of the experimental data are reasonably reproduced for the differential cross sections and some spin observables of the np and pp scattering. Predictions for the Σ^+p and Λp scattering observables at intermediate energies are very much model-dependent, suggesting the importance of further experimental studies on these quantities.

13.75.Cs,12.39.Jh,13.75.Ev,24.85.+p

Typeset using REVTEX

*JSPS Postdoctoral Fellow.

I. INTRODUCTION

The nucleon-nucleon (NN) and hyperon-nucleon (YN) interactions are among the most important fundamental interactions which result from highly non-trivial dynamics of quarks and gluons, governed by quantum chromodynamics (QCD). Since QCD is not amenable to the direct solution of low-energy hadron phenomena, QCD-inspired effective quark models are usually employed to study these interactions. The composite nature of the nucleon and hyperon is taken into account most straightforwardly in the resonating-group method (RGM). In the simplest RGM formulation for the NN interaction [1], the effective quark-quark (qq) interaction is usually built by combining a phenomenological quark-confining potential with a one-gluon exchange potential through the color analog of the Fermi-Breit (FB) interaction. This simple $(3q)$-$(3q)$ model could elucidate only the extreme short-range part of the NN interaction, which was found to be purely repulsive. Since the long-range part of the interaction is dominated by meson-exchange effects, any RGM description in the simple $(3q)$-$(3q)$ model must comprise effective meson-exchange potentials (EMEP) introduced by some appropriate means.

Meanwhile, many successful meson-exchange descriptions of the NN interaction have been extended to the YN interaction. These include several versions of the one-boson exchange potentials (OBEP) such as the Nijmegen models [2–4] and the Jülich potentials. [5,6] In these models a large number of baryon-meson coupling constants are constrained by the use of the SU_3 relations, and several SU_3 parameters are determined to reproduce the NN properties together with the low-energy cross-section data for the YN scattering. One can inherit many techniques developed here for incorporating EMEP in the quark model. The extension of the $(3q)$-$(3q)$ RGM study of the NN interaction to the YN interaction is, however, by no means straightforward, since the lack of the medium-range attraction in the quark model leads to too much ambiguity in the way of supplementing EMEP. Furthermore, in the study of the YN interaction, the flavor-symmetry breaking should be correctly introduced even though we choose the spin-flavor SU_6 symmetry as a starting point.

We have recently achieved a simultaneous description of the NN and YN interactions in the RGM formulation of the spin-flavor SU_6 quark model [7,8]. This formulation incorporates EMEP induced from the scalar (S) and pseudoscalar (PS) meson nonet exchanges at the quark level, and calculates the spin-flavor factors of the quark-exchange kernel explicitly by assuming the Gell-Mann matrices for the flavor operators of the octet-meson exchange potentials. Since the hyperon and the nucleon belong to the same class of the spin-flavor SU_6 supermultiplet $\underline{56}$, the spin-flavor factors thus evaluated give a strong constraint for the parameters of the EMEP. The microscopic approach to introduce EMEP at the quark level gives strong correlation among different flavor channels of the NN and YN interactions, making it possible to utilize the very rich experimental information of the NN interaction for the study of the YN interaction with scarce experimental information. In [7,8] we have fixed model parameters by using some appropriate NN properties and the available low-energy "total" cross section data for the YN scattering, and found that the deuteron properties and the NN phase shifts up to the partial waves $J \leq 4$ are reasonably reproduced, as well as the low-energy YN differential cross sections. In [9] we have shown that, for some particular energies, reasonable agreement with the experimental data is obtained not only for the total and differential cross sections but also for some spin observables of the np and pp systems. A similar analysis is also carried out in [10] for $\Sigma^+ p$ scattering at $p_\Sigma = 450$ MeV/c, in which a strong correlation between the resonance behavior of various OBEP models and the predicted differential cross sections and polarization is discussed.

In this investigation, we further continue our study of the scattering observables of the NN and YN systems. The reason why we need to examine the scattering observables in addition to the phase shifts is as follows:

1) In the YN system, the phase-shift analysis does not seem to be possible even in future, because of the very poor statistics of the experimental data.

2) In the NN system where the phase-shift analysis exists, we can learn the quality of our model predictions for reproducing the experimental data. This information is

indispensable, when we try to analyze future YN data by using our quark model.

3) Since our quark model is not perfect in reproducing the NN phase shifts, it is useful to pinpoint the flaw of the predicted scattering observables for the future renovation of our quark model.

It is certainly true that the characteristics of the interaction pieces are usually reflected more clearly in the behavior of the phase shifts as long as the energy is not high. In the studies of the YN interaction by the OBEP models, however, the combined discussion of the phase-shift behavior and the scattering observables is not frequently done, since the parameters of OBEP's are supposed to embody the characteristics of the experimental data. In the present framework, the short-range part of the NN and YN interactions is uniquely determined. It would be useful to examine the correlation between the characteristics of the phase-shift behavior and those of the scattering observables by taking advantage of the strong correlation of the NN and YN interactions in our quark model.

We stress that our purpose in studying the NN and YN interactions in the quark model is not actually to reproduce the experimental data, but to clarify the various aspects of the baryon-baryon interactions, which reflect dynamical processes taking place between the composite systems of quarks. In the present approach, these processes are dominated by the effective qq interaction as well as important kinematical requirements arising from the quark Pauli principle and the symmetries of the spin, flavor, and color degrees of freedom. In particular, it is a great advantage of the RGM framework that we can deal with the NN and YN interactions on an equal footing as long as we assume the SU_6 wave functions for the baryons and a unique qq interaction between quarks. In our quark-model study, the perfect reproduction of the experimental data of the NN system is not a mandatory condition to proceed to the study of the scattering observables of the YN system, but more important is that the properties directly related to the characteristics of the interaction are qualitatively reproduced. We expect that these properties are reflected in the energy dependence and shapes of the angular distributions of various scattering observables. Since the

present discrepancies between the predicted and empirical NN phase shifts cannot be easily overcome by a mere change of the parameter values, we deem that the expected discrepancies between the calculated and experimental scattering observables should be used for the future feedback to the improvement of the present quark model or the present framework.

This viewpoint is largely different from those of previous quark-model studies of the NN scattering observables. For example, the Paris group [11] combined the quark-model potential [12] with the long- and medium-range part of the Paris potential, by introducing a special type of cutoff function. They tested the quality of the model by confronting its predictions directly with data on scattering observables, and found that the fit to the existing pp data was not satisfactory. It is not appropriate, however, to substitute the quark-model potential for the short-range part of the Paris potential. One should allow the quark model the freedom to choose an optimum framework for the EMEP. Another calculation of the spin observables by the Tübingen-Salamanca group [13,14] is motivated by the hope that one could find an additional information on the quark degrees of freedom at short distances. They also try to estimate the quality of the quark-model predictions for the polarization observables in the NN system. The extension to the YN system is their future work.

In this paper, we first extend our work in [9] and examine the energy dependence of the NN scattering observables up to about 300 MeV. This is a necessary step to make sure that our quark model has attained essential ingredients which enable us to describe the characteristic features of the NN and YN interactions up to certain incident energies. Since a detailed discussion of the Σ^+p scattering observables at the intermediate energies is already made in [10], we briefly mention characteristics of the various models, which appear in the energy-dependence of the the differential cross sections and polarization. Next we proceed to analyze the Λp system, for which new experimental data are expected from KEK in the near future. In this system the coupling with the $\Sigma N(I = 1/2)$ channel through the antisymmetric LS force ($LS^{(-)}$ force) is particularly important at the cusp region, although we remain in this paper in the energy region where the ΣN channel is still closed. The result of our preceding model, RGM-F [15–17], is mentioned only briefly when some difference from

FSS and RGM-H appears.

In the next section we formulate the model to calculate the NN and YN scattering observables. After a brief discussion of our quark model, the procedure to calculate the scattering observables from the S-matrix is outlined. Section III deals with results and discussions. The differential cross sections and the spin observables of the np and pp scattering are examined in Sec. III A, those of the Σ^+p scattering in Sec. III B, and those of the Λp scattering in Sec. III C. The final section is devoted to a summary.

II. FORMULATION

A. Quark model

Here we only recapitulate some important features of our quark model. Our new versions, FSS [7,8] and RGM-H [8], and their preceding version RGM-F [15–17] are formulated in the $(3q)$-$(3q)$ RGM applied to the system of two $(0s)^3$ clusters, where the quark interaction is composed of the full FB interaction with explicit quark-mass dependence, a simple confinement potential of quadratic power law, and EMEP acting between quarks. The RGM equation derived from the variational principle $\langle \delta\Psi | E - H | \Psi \rangle = 0$ is formulated for the parity-projected relative wave function $\chi^\pi(R)$ as [8]

$$\left[\varepsilon_\alpha + \frac{\hbar^2}{2\mu_\alpha} \left(\frac{\partial}{\partial \boldsymbol{R}} \right)^2 - \sum_\beta V_{\alpha D}^{(CN)\beta}(\boldsymbol{R}) - \sum_\beta V_{\alpha D}^{(SS)\beta}(\boldsymbol{R}) - \sum_\beta V_{\alpha D}^{(TN)\beta}(\boldsymbol{R})\,(S_{12})_\alpha \right] \chi_\alpha^\pi(\boldsymbol{R})$$
$$= \sum_{\alpha'} \int d\boldsymbol{R}' \left[\sum_\Omega \mathcal{M}_{\alpha\alpha'}^{(\Omega)}(\boldsymbol{R}, \boldsymbol{R}') - \varepsilon_\alpha\, \mathcal{M}_{\alpha\alpha'}^{N}(\boldsymbol{R}, \boldsymbol{R}') \right] \chi_{\alpha'}^\pi(\boldsymbol{R}') \ , \qquad (1)$$

where ε_α is the relative energy in the channel α. Each channel is specified by a set of quantum numbers $\alpha = [1/2(11)a_1, 1/2(11)a_2]\ SS_zYII_z; \mathcal{P}$, where $\mathcal{P}$ is the flavor-exchange symmetry phase [15]. The summation over Ω for the exchange kernel $\mathcal{M}_{\alpha\alpha'}^{(\Omega)}$ involves not only the exchange kinetic-energy (K) term, but also various pieces of the FB interaction, as well as several components of EMEP. The FB interaction involves the color-Coulombic (CC) piece, the momentum-dependent Breit retardation (MC) piece, the color-magnetic (GC) piece, the

symmetric LS (sLS) piece, the antisymmetric LS (aLS) piece, and the tensor (T) piece. The EMEP contribution, on the other hand, yields the central (CN) component from the S-mesons, and the spin-spin (SS) and tensor (TN) terms originating from PS mesons. These terms are further divided into contributions from some particular meson species denoted by β, which is explicitly shown in Eq. (1) only for the direct potentials.

The difference of the three versions lies solely in the meson species, the interaction types, and the treatment of the spin-flavor factors for the EMEP assumed to act between quarks. In RGM-F the one-pion exchange and K-meson exchange tensor forces are only taken into account, in addition to the S-meson nonet (ϵ, S^*, δ and κ) exchanges, while in FSS and RGM-H all pieces of the PS-meson nonet (η', η, π and K) are introduced with respect to the spin-spin and tensor terms. Coupling constants of these mesons to quarks are controlled by the SU_3 coupling constants appearing in the direct term of the RGM equation, and are determined to realize an optimum fit to some of the NN properties and available low-energy "total" cross sections for the YN scattering. The NN properties fitted are the deuteron binding energy, $^1S_0$ scattering length for np (FSS) or pp (RGM-H) scattering, and S- and P-wave phase shifts up to about 200 MeV, adjusted to the recent phase-shift analysis by the Nijmegen group [18]. Since Table III of [8] has a misprint for f_1^{PS} and f_8^{PS} of RGM-H, we show correct model parameters of FSS and RGM-H in Table I.

The spin-flavor factors of the EMEP are not explicitly calculated in RGM-F. In this model the exchanged mesons are first assumed to be flavor-singlet, and then the overall strength is adjusted such that the flavor dependence of the spin-flavor factors in the direct term correctly reproduces the flavor dependence of the Nijmegen model-F, which is determined from the products of the baryon-meson coupling constants with the SU_3 relations. For scalar mesons the strength of the original model-F parameters are multiplied with a common reduction factor, $c_{+1} = 0.56$ for the flavor symmetric states with $\mathcal{P} = +1$ or $c_{-1} = 0.4212$ for the flavor antisymmetric states with $\mathcal{P} = -1$. These are determined to reproduce the $^1S_0$ phase shift of the NN scattering and the correct binding energy of the deuteron. On the other hand, the spin-flavor factors of EMEP are explicitly calculated in FSS and RGM-H. We have

found that the full microscopic approach in these models imposes too strict a constraint on the SU_3 EMEP parameters. For example, the $F/(D+F)$ ratio of the flavor octet mesons is no longer a free parameter, but takes specific SU_6 values originating from the SU_6 spin-flavor wave functions of the octet baryons. The pure electric nature of the S-mesons with $\alpha_S = 1$ leads to a difficulty that the direct potentials for the ΛN and ΣN systems become identical. Under this constraint it is not easy to ensure an appropriate relative strength of the central attraction between ΛN and ΣN channels. In particular the central attraction of the $\Sigma^+ p$ channel is usually too strong, if we fix that of the ΛN channel to fit the low-energy Λp cross sections. In FSS we avoid this difficulty by choosing a little larger value of θ_S for the isoscalar meson mixing only for the $\Sigma N(I = 3/2)$ system. In RGM-H we partially return to the old prescription of RGM-F and revise a degree of freedom of α_S by using the approximate spin-flavor-color factors only for the isoscalar S-mesons ϵ and S^*.

A short comment follows for the spin-spin part of the PS meson exchange potentials and their coupling constants. The spin-spin part includes the delta-function type contact term which is recently advocated by some authors [20] as a replacement of the color-magnetic term of the FB interaction. In fact this term also yields the short-range repulsion in the S-wave channels of the NN interaction. However, we are reluctant to take this contact term of EMEP as the origin of the very intricate flavor dependence of the baryon-baryon interaction. We have introduced a common reduction factor c_δ for this term and determined the value in the NN system. In our previous formulation [8], we included the factor $m_\beta/m_{\pi^+})^2$ common to the spin-spin and tensor terms of the PS meson exchange potentials. In the actual calculation of FSS and RGM-H, however, this mass factor is introduced only for the spin-spin term.

B. Scattering observables

We solve the coupled-channel RGM equation Eq. (1) by the variational method, employing Gaussian-type trial functions [21]. The S-matrix thus obtained constitutes essential

constructing blocks for the scattering amplitude which is expressed by eight invariant amplitudes $a, \cdots, h$ [22]:

$$M = \frac{1}{2}\{(a+b) + (a-b)(\sigma_1 \cdot \boldsymbol{n})(\sigma_2 \cdot \boldsymbol{n}) + (c+d)(\sigma_1 \cdot \boldsymbol{m})(\sigma_2 \cdot \boldsymbol{m}) + (c-d)(\sigma_1 \cdot \boldsymbol{l})(\sigma_2 \cdot \boldsymbol{l}) + e(\sigma_1 + \sigma_2) \cdot \boldsymbol{n} + f(\sigma_1 - \sigma_2) \cdot \boldsymbol{n} + g\{(\sigma_1 \cdot \boldsymbol{l})(\sigma_2 \cdot \boldsymbol{m}) + (\sigma_1 \cdot \boldsymbol{m})(\sigma_2 \cdot \boldsymbol{l})\} + h\{(\sigma_1 \cdot \boldsymbol{l})(\sigma_2 \cdot \boldsymbol{m}) - (\sigma_1 \cdot \boldsymbol{m})(\sigma_2 \cdot \boldsymbol{l})\}\} \quad , \tag{2}$$

where

$$\boldsymbol{l} = \frac{\boldsymbol{k}_f + \boldsymbol{k}_i}{|\boldsymbol{k}_f + \boldsymbol{k}_i|} \quad , \quad \boldsymbol{m} = \frac{\boldsymbol{k}_f - \boldsymbol{k}_i}{|\boldsymbol{k}_f - \boldsymbol{k}_i|} \quad , \quad \boldsymbol{n} = \frac{\boldsymbol{k}_i \times \boldsymbol{k}_f}{|\boldsymbol{k}_i \times \boldsymbol{k}_f|} \quad , \tag{3}$$

and $\boldsymbol{k}_i$ and $\boldsymbol{k}_f$ are unit vectors of the incident and scattered particles in the center-of-mass (c.m.) system. The partial-wave expansion of the invariants amplitudes are given in Eq. (3) of [23] for $a, \cdots, e$, and in Eq. (2.21) of [22] for f, g, h. The last three amplitudes, f, g and h, do not appear for the NN scattering, since the process is invariant under the exchange of two particles (f and h) and the time reversal (g and h). The time reversal property also excludes g and h even in the elastic YN scattering. These three terms correspond to the non-central forces characteristic in the YN scattering; i.e, f corresponds to $LS^{(-)}$, g to $S_{12}(\boldsymbol{r}, \boldsymbol{p})$, and h to $LS^{(-)\sigma}$ (i.e., the $(\boldsymbol{L} \cdot \boldsymbol{S}^{(-)})P_\sigma$ term), respectively [24]. In particular, $LS^{(-)}$ and $LS^{(-)\sigma}$ interactions involve the spin change between 0 and 1, together with the transition of the flavor-exchange symmetry $\mathcal{P} \neq \mathcal{P}'$. In the NN scattering this is forbidden from the isospin conservation, since the flavor-exchange symmetry is uniquely specified by the isospin: $\mathcal{P} = (-1)^{1-I}$. On the other hand, these interactions are all possible when ΛN-ΣN transition is incorporated in the YN scattering, leading to intriguing interplay of non-central forces.

The standard procedure to derive the polarization observables of the NN and YN scattering is formulated in terms of the spin density matrix given by

$$\rho_{\{\substack{\text{inc}\\\text{scat}}\}} = (\mathrm{Tr}\rho_{\{\substack{\text{inc}\\\text{scat}}\}}) \frac{1}{4} \sum_{\mu\nu} \overline{\langle \sigma_{1\mu}\sigma_{2\nu} \rangle}_{\{\substack{\text{inc}\\\text{scat}}\}} \sigma_{1\mu}\sigma_{2\nu} \quad , \tag{4}$$

where, $\mu, \nu = 0, l, m, n$, denote the components of the spin vectors of the first and second particles with respect to the unit vectors, $\boldsymbol{l}$, $\boldsymbol{m}$, $\boldsymbol{n}$, in Eq. (3). When the polarization of the particle $i = 1$ or 2 is not measured, we assume $\mu, \nu = 0$ and $\sigma_{i0} = 1$. The density matrix of the spin variables in the outgoing channel is related to that in the incident channel through $\rho_{scat} = M\, \rho_{inc}\, M^\dagger$. The differential cross section is given by

$$\frac{d\sigma}{d\Omega} = \frac{\mathrm{Tr}\rho_{scat}}{\mathrm{Tr}\rho_{inc}} = \sigma_0(\theta) \sum_{\mu\nu} X_{00\mu\nu} \overline{\langle \sigma_{1\mu}\sigma_{2\nu} \rangle}_{inc} \quad , \tag{5}$$

where $\sigma_0(\theta) = (1/4)\,\mathrm{Tr}\left[MM^\dagger\right]$ is the differential cross section when the incident and target particles are both unpolarized. In Eq. (5) the polarization matrix $X_{\kappa\lambda\mu\nu}$ is defined by

$$\sigma_0(\theta)\, X_{\kappa\lambda\mu\nu} = \frac{1}{4}\,\mathrm{Tr}\left[\sigma_{1\kappa}\sigma_{2\lambda}\, M\, \sigma_{1\mu}\sigma_{2\nu}\, M^\dagger\right] \quad . \tag{6}$$

Any polarization observables in the c.m. system can be calculated from the polarization matrix Eq. (6) through

$$\overline{\langle \sigma_{1\kappa}\sigma_{2\lambda} \rangle}_{scat} \frac{d\sigma}{d\Omega} = \sigma_0(\theta) \sum_{\mu\nu} X_{\kappa\lambda\mu\nu} \overline{\langle \sigma_{1\mu}\sigma_{2\nu} \rangle}_{inc} \quad . \tag{7}$$

From the definition Eq. (6), it is clear that all together $4^4 = 256$ matrix elements of $X_{\kappa\lambda\mu\nu}$ are expressed as linear combinations of real 64 products, $|a|^2, |b|^2, \cdots, \Re e[a^*b], \Im m[a^*b], \cdots$. An elegant procedure to derive all the explicit expressions of 64 independent observables as the linear combinations of these is given by Bystricky, Lehar and Winternitz [25] in their formulation of the theory of scattering observables for the NN system. The final result for the most general scattering amplitude Eq. (2) involving spin-1/2 particles is tabulated in Table I of [22].

The transformation of the spin observables expressed in the unit vectors, $\boldsymbol{l}$ and $\boldsymbol{m}$, in the c.m. system to those expressed in the body-fixed frame in the laboratory system involves not only a trivial kinematical rotation around the $\boldsymbol{n}$ axis, but also an extra rotation around the same axis, which is called by Stapp [26] the relativistic rotational correction of the polarization vectors. The angles, Ω_L and Ω_R, by which the polarization vectors of the scattered and recoil particles are rotated, respectively, are obtained as a result of three

successive Lorentz transformations with non-parallel velocity vectors [6,26,27]. The spin observables in the laboratory system, incorporating these relativistic corrections, are also given in Table II of [22] in the most compact form. The relationship between α, β in Eq. (3.8) of [22] and Ω_L, Ω_R in Eq. (B.7) of [6] is given by

$$\alpha = \Omega_L - \frac{\theta}{2} + \theta_L \ , \qquad \beta = \Omega_R + \pi - \frac{\theta}{2} - \theta_R \ , \tag{8}$$

where θ_L (θ_R) is the scattering (recoil) angle in the laboratory system and θ is that in the c.m. system. For the elastic scattering, the simple relations $\Omega_L = \theta - 2\theta_L = 2\alpha$ and $\Omega_R = -\pi + \theta + 2\theta_R = -\pi + 2\beta$ hold [6].

III. RESULTS AND DISCUSSIONS

A. NN scattering

In this subsection we discuss scattering observables of the NN system predicted in the present quark model. Since the model parameters are fixed by fitting the S-wave and P-wave phase shifts up to the energy range $T_{lab} \leq 200$ MeV, the low-energy scattering observables are naturally well reproduced. However, the phase shifts of higher partial waves are only qualitatively reproduced. For example, in FSS and RGM-H (and also in RGM-F) the $^3D_2$ phase shift is too attractive by more than 10° in the energy range 200 MeV $\sim$ 300 MeV [8], which seems to be a common feature of most quark-model calculations (see, for example, [12]). The deviation of the ϵ_2 mixing parameters of the $^3P_2$ - $^3F_2$ coupling is not small either. These features indicate some insufficiency of the present model in the tensor and/or quadratic LS components, which may be related to our assumption of no vector mesons included.

The differential cross sections ($d\sigma/d\Omega$) and the polarization (P) for the np scattering, predicted by our quark model, are displayed in Fig. 1, and those for the pp scattering in Fig. 2. Solid curves indicate results by RGM-H and dashed curves by FSS. The partial waves up to the total angular momentum $J_{\max}$=7 are taken into account. The comparison with the

experimental data [28] shows that qualitative agreement is achieved in these cases. In the np scattering, the differential cross section data show typical V-shape behavior. The peak position for the polarization data is enhanced and moves gradually to the forward angles as the incident energy increases. Our quark model reproduces these features quite well. There are, however, some deviations from the experimental data at higher energies. In the differential cross sections, our quark model gives slightly too large values at $\theta_{\rm c.m.} \leq 30°$ and yields a bump structure around $\theta_{\rm c.m.} = 130°$. Some deviations from the experimental data, especially at $\theta_{\rm c.m.} = 30°$ - $60°$ and $\theta_{\rm c.m.} = 90°$ - $150°$, are also seen in the polarization at 310 MeV. For the pp scattering in Fig. 2, the differential cross sections and the polarization are plotted only for $\theta_{\rm c.m.} \leq 90°$, since these are repeated for $\theta_{\rm c.m.} = 90°$ - $180°$. Although our model (especially FSS) slightly overestimates the differential (and consequently "total") cross sections, a reasonable description is still obtained with respect to the energy dependence and the shape of the angular distribution. The model RGM-H gives a slightly better fit to the experimental differential cross sections, since the parameters of this model are fixed by using the pp phase shifts with $I = 1$. The measured polarization becomes larger as the energy increases. Our quark model reproduces this energy dependence for the magnitude of the polarization. The polarization on the high-energy side ($T_{\rm lab} \sim 213$ MeV) is slightly underestimated.

The quality of the agreement with the experiment is similar even for the other spin observables. Figures 3 (np) and 4, 5 (pp) show the comparison of the depolarization D and the Wolfenstein parameters, R, R' and A. These spin observables do not have a simple symmetry property with respect to the scattering angles even for the pp system.

Next we briefly discuss the improvement of the scattering observables in RGM-H and FSS over those in their preceding version RGM-F. In the polarization and the depolarization at 50 MeV, we do not find any large deviation among these calculations. On the other hand, the differential cross sections and the spin correlation parameters of RGM-F deviate from the experimental data at backward angles, whereas those of RGM-H and FSS give better results. (See Fig. 1(b) of [9] for the differential cross sections at 90 MeV.) We attribute this difference

to the lack of the spin-spin term of the PS mesons (especially, the pion) in the RGM-F. It is interesting to note that this deviation appears only in the differential cross sections and the spin correlation parameters, and not in the polarization and the depolarization. This may indicate that some observables are very sensitive to the particular components of the interaction. In the Σ^+p system we will see another example of this kind of property with respect to the resonance behavior of particular partial waves.

Summarizing this subsection, we have found that the present quark model can qualitatively reproduce very rich experimental data of the NN scattering observables at the wide energy range up to $T_{\rm lab} \lesssim 300$ MeV. Although the quality of the fit is far behind the OBEP approach, the essential ingredients of the NN interaction can be incorporated in our quark model, as long as this energy region is concerned. This is a necessary condition for the purpose of extending the present model to the YN interaction. Some deviations from the experimental data found on the high-energy side should be investigated for the improvement of the present framework.

B. Σ^+p scattering

The SU_3 content of the Σ^+p system is (22) for the flavor-symmetric ${}^1E$ and ${}^3O$ states and (30) for the flavor-antisymmetric ${}^3E$ and ${}^1O$ states. [15] Since the pp system also has the SU_3 symmetry (22), the Σ^+p interaction in the ${}^1E$ and ${}^3O$ states is expected to resemble the well-known pp interaction as long as the qq interaction is approximately SU_3 scalar. On the other hand, the Σ^+p interaction in the ${}^3E$ and ${}^1O$ states is a priori unknown from this kind of simple symmetry discussion. In the quark model, the most compact $(0s)^6$ configuration of the $\Sigma N(I = 3/2)$ ${}^3S_1$ state is almost forbidden by the effect of the Pauli principle. The Σ^+p interaction in the ${}^3S_1$ state is consequently repulsive due to this kinematical effect arising from the quark structure of the baryons. On the other hand, the Pauli effect gives weak attraction for the ${}^1P_1$ state through the kinetic-energy exchange kernel in the RGM formalism. [15]

In the OBEP models, the phase-shift behavior of the ${}^3S_1$ and ${}^1P_1$ states at $p_\Sigma \geq 300$ MeV/c is very much model-dependent, which results in different predictions of the differential cross sections and polarization at intermediate energies [10]. For example, the ${}^1P_1$ phase shift of the Nijmegen hard-core model-F (HC-F) [3] and model-D (HC-D) [2] shows strong resonant behavior around 400 MeV/c, which yields strong enhancement of the differential cross sections at the forward and backward angles. The Nijmegen soft-core model (NSC) [4], on the other hand, shows a broad resonance structure around 600 MeV/c in the ${}^3S_1$ phase shift, although it is repulsive below $p_\Sigma \leq 400$ MeV/c. The small phase-shift values in the ${}^3S_1$ state around this energy result in small values of the differential cross sections and the polarization . The Jülich models [5,6] also have a broad ${}^3S_1$ resonance, resulting in very small differential cross sections at 450 MeV/c [10].

These features of scattering observables can be clearly seen in Fig. 6, which displays the energy dependence of the Σ^+p differential cross sections and polarization up to $p_\Sigma =$ 800 MeV/c. The predictions by RGM-H (solid curve), FSS (dashed curve), the Nijmegen HC-F (crosses), and NSC (circles) are displayed. All the models give similar results up to 200 MeV/c, except for some overestimate of the differential cross sections in RGM-H. At higher energies, characteristic features of individual models appear. The ${}^1P_1$ resonance in HC-F is reflected in the V-shape behavior of the differential cross sections. The ${}^3S_1$ resonance in NSC gives very small values of the the differential cross sections for $p_\Sigma = 400$ - 600 MeV/c. The polarization is also sensitive to the resonance structure of the ${}^3S_1$ phase shift. For example, in NSC it stays at small values below 600 MeV/c. The two versions of our quark model predict a behavior very similar to each other for both of these observables. We have also compared these model predictions with the recent experimental data from KEK for the Σ^+p differential cross sections averaged over the energy range $p_\Sigma = 300$ - 600 MeV/c [29]. Unfortunately the poor statistics of the data obtained so far does not lead to any meaningful conclusion on the characteristics of the Σ^+p interaction in the ${}^3E$ and ${}^1O$ states. Further experimental investigations of the differential cross sections and polarization at the intermediate energies are surely very important to understand this interaction.

C. Λp scattering

In this subsection, we discuss scattering observables of the Λp interaction based on the analysis of the phase-shift behavior of the ΛN - $\Sigma N(I = 1/2)$ coupled-channel calculation. It is found in [8] that the channel coupling effect between the ΛN and $\Sigma N(I = 1/2)$ channels is very important even below the ΣN threshold at $p_\Lambda = 638$ MeV/c (which corresponds to the Λ-Σ mass difference $\Delta E_{\Lambda-\Sigma} = 77.49$ MeV). This situation is naturally understood in the quark model, since two SU_3 states, $(11)_a$ and $(11)_s$, which newly appear in this system, are largely mixed in the ΛN system. In particular, the flavor symmetric $(11)_s$ state is completely forbidden in the most compact $(3q)$-$(3q)$ configuration, which leads to the strong repulsion to the $^1S_0$ state of the $\Sigma N(I = 1/2)$ system. On the other hand, $^1S_0$ state of the ΛN system contains the (22) component with 90 %, resulting in the attractive feature of the phase shift with the short-range repulsion, similar to the the $NN(I = 1)$ system. The $^3S_1$ states of the ΛN and $\Sigma N(I = 1/2)$ systems both contain the (03) and $(11)_a$ components fifty-fifty, so that one may expect their interactions should be very similar to each other so long as the total Hamiltonian is approximately SU_3 scalar. It is, however, possible that this observation found in [15] for the central interaction is largely violated by the strong effect of the flavor symmetry breaking, especially by the π- and K-meson exchange tensor force. In the ΛN system, the one-pion exchange tensor force becomes important only through the coupling with the ΣN channel, whereas it should give an appreciable contribution to the ΣN system. It is, therefore, important to determine the strength of the attraction affecting the ΛN and $\Sigma N(I = 1/2)$ systems in the $^3S_1$ (and also $^1P_1$) state independently.

Another characteristic feature of the ΛN - $\Sigma N(I = 1/2)$ system is the the $(11)_a$ - $(11)_s$ transition due to the $LS^{(-)}$ force. This effect of the flavor-exchange symmetry for the interchange of the two particles is accompanied with the spin transition between 0 and 1. The spin values are not conserved any more in the YN system and ^1J_J state is coupled with ^3J_J state through the $LS^{(-)}$ force. Although the $LS^{(-)}$ force exists even in the Σ^+p system, the different SU_3 contents of the ^3O and ^1O states (which are (22) and (30), respectively)

make the transition very weak, as long as the total Hamiltonian is almost SU_3 scalar with small flavor symmetry breaking. On the other hand, we have found in [7,8] that the $LS^{(-)}$ force originating from the Fermi-Breit interaction between quarks plays a very important role to enhance the cusp structure of the Λp elastic cross sections at the ΣN threshold. This is particularly prominent in the model FSS, where the resonance structure in the $\Sigma N(I = 1/2)$ $^3P_1$ state is moved to the ΛN $^1P_1$ state due to the very strong coupling by the $LS^{(-)}$ force. We will show below another effect of this coupling in the polarization observables.

Figures 7 and 8 show the differential cross sections ($d\sigma/d\Omega$), the depolarization (D), the polarization of the scattered (P_Λ) and recoil (P_N) particles for the Λp elastic scattering with respect to various incident momenta of the Λ-particle below the ΣN threshold. The solid curve denotes predictions by RGM-H and the dashed curve by FSS. For comparison, predictions by some standard OBEP models, the Nijmegen NSC and the Jülich model-B (Jülich B), are also shown by circles and diamonds, respectively. We first note that the predictions by FSS and RGM-H are characteristically very similar to each other, except for the stronger enhancement of the differential cross sections in FSS near the ΣN threshold. This enhancement is apparently related to the fact that the $LS^{(-)}$ coupling is stronger in FSS than in RGM-H. If we compare the predictions of D and P_Λ by various models at $p_\Lambda = 600$ MeV/c, we find that the difference between FSS and RGM-H is smaller than the difference between the two OBEP models. Since predictions of full Wolfenstein parameters by various OBEP models are already given at this particular incident momentum, we also give our predictions for R, R', A and A' in Fig. 9. We find that these quantities are strongly model-dependent. Even our quark model predicts different results between FSS and RGM-H, which is also related to the different coupling features of the ΛN and $\Sigma N(I = 1/2)$ channels by the $LS^{(-)}$ force. This difference between FSS and RGM-H sometimes exceeds the difference from the other two OBEP models. Much experimental information is required to predict these quantities without ambiguity.

Since the structure of the ΛN interaction is rather complicated, it is necessary to clarify various aspects of the interaction step by step. First let us discuss the S-wave phase shifts

and their effect on the scattering observables. Although all the models for the YN interaction are made such that the empirical low-energy Λp total cross sections in 120 - 330 MeV/c region [30,31] are reproduced, there still remains much ambiguity in the relative strength of the attraction appearing in the $^1S_0$ and $^3S_1$ phase shifts. Table II shows the $^1S_0$ and $^3S_1$ phase-shift values predicted by various models at $p_\Lambda = 200$ MeV/c, where they reach almost maximum values. The effective-range parameters are also shown for comparison. These models are classified into two categories; one gives a small difference between the $^1S_0$ and $^3S_1$ phase shifts and the other gives a larger value for $^1S_0$ and a smaller one for $^3S_1$. All the OBEP models and RGM-F[1] belong to the first category and our new version of the quark model, FSS and RGM-H, belong to the second one. In usual the $^1S_0$ state is more attractive than the $^3S_1$ state, except for the Nijmegen model-D and RGM-F. This feature is required from the analysis of the energy spectra of light Λ hypernuclei. First the hypertriton ${}^3_\Lambda$H is bound, while ${}^3_\Lambda$He is not. Secondly ${}^4_\Lambda$H and ${}^4_\Lambda$He have the 0^+ ground state and an excited state 1^+ at about 1 MeV. The determination of the relative strength of the attraction in the $^1S_0$ and $^3S_1$ states is, therefore, very crucial for understanding the detailed structure of light Λ hypernuclei.

The two categories could be characterized by the depolarization D. If we retain only the S-wave in the low-energy limit, D is explicitly calculated from

$$D \sim \frac{2\,[(\sin\delta_t)^2 + \sin\delta_s\,\sin\delta_t\,\cos(\delta_s - \delta_t)]}{(\sin\delta_s)^2 + 3(\sin\delta_t)^2}\quad , \tag{9}$$

[1]In [16,17], the K-meson coupling constants, $f_{N\Lambda K}$ and $f_{N\Sigma K}$, for the tensor term are inadvertently taken to be the electric-type coupling constants of the K^* mesons; i.e., $f_{N\Lambda K^*} = -1.37177$ and $f_{N\Sigma K^*} = 0.79199$, instead of the correct values $f_{N\Lambda K} = -4.30263$ and $f_{N\Sigma K} = -0.77317$. By this change, the $^3S_1$ phase shift of the Λp channel in RGM-F becomes more attractive than that of the $^1S_0$ state. The Λp total cross section at $p_\Lambda = 200$ MeV/c (given in Fig. 14 of [17]) has increased about 45 %, but is still within the experimental error bars. The correct effective range parameters for the $^3S_1$ phase shift in RGM-F are given in Table II.

where $\delta_s = \delta(^1S_0)$ and $\delta_t = \delta(^3S_1)$. If $\delta_s = \delta_t$, Eq. (9) yields $D = 1$. At $p_\Lambda = 100$ MeV/c, the phase-shift values of each model give $D \sim 1$ for the Nijmegen model-D and RGM-F, and much smaller values 0.55 for FSS and 0.56 for RGM-H. The Nijmegen soft-core model NSC gives 0.93. The depolarization behavior in Fig. 7 clearly shows that this situation continues up to about 200 - 300 MeV/c.

Once the incident energy becomes higher, the P-wave contribution becomes important. It is still not clear if the P-wave ΛN interaction is repulsive or attractive. The experimental data for the low-energy angular distribution seems to indicate that it is slightly attractive [30,31], although these data involve large error bars. The central components in the single-channel P-wave phase shifts of the ΛN scattering are generally repulsive in our quark model. After introduction of the non-central forces, the $^3P_0$ phase shift becomes repulsive and the $^3P_2$ phase shift becomes attractive mainly by the LS force. Table III shows the P-wave phase shifts of FSS and RGM-H in the full coupled-channel calculation with respect to the incident momenta below the ΣN threshold. The mixing angles ρ_1 between $^1P_1$ and $^3P_1$ channels by the $LS^{(-)}$ force are also shown in the standard notation of bar phase shifts. Here we clearly find that the mixing is stronger in FSS than in RGM-H. As the energy approaches the ΣN threshold, both of the $^1P_1$ and $^3P_1$ phase shifts obtain appreciable attraction by the effect of the step-like resonance in the $^1P_1$ state of FSS and of the dispersion-like resonances otherwise [8]. Except for this quantitative difference of the coupling features near the ΣN threshold, FSS and RGM-H yield very similar results for the P-wave phase shifts of the ΛN elastic scattering.

In order to see the contributions of the P-wave components more clearly, we examine the forward-to-backward ratio F/B of the Λp angular distributions for the energy range $p_\Lambda \leq$ 300MeV/c. If we keep the dominant S-wave phase shifts, δ_s and δ_t, and small corrections, ϵ_1, $\delta_s^1 = \delta(^1P_1)$, $\delta_t^J = \delta(^3P_J)$ with $J = 0,\ 1,\ 2$, the total differential cross sections are approximated by

$$\sigma_0(\theta) \sim \left[\frac{1}{4}(\sin\delta_s)^2 + \frac{3}{4}(\sin\delta_t)^2\right] + \left[\frac{3}{2}\sin\delta_s\,\sin\delta_s^1\,\cos(\delta_s - \delta_s^1)\right.$$

$$+\frac{1}{2}\sin\delta_t\,\sin\delta_t^0\,\cos(\delta_t-\delta_t^0)+\frac{3}{2}\sin\delta_t\,\sin\delta_t^1\,\cos(\delta_t-\delta_t^1)$$
$$+\frac{5}{2}\sin\delta_t\,\sin\delta_t^2\,\cos(\delta_t-\delta_t^2)\Big]\,\cos\theta\ . \qquad (10)$$

Apparently, the attractive feature of the P-wave phase shifts gives an F/B ratio greater than one. Note that the effect of ϵ_1 disappears in this approximation. We find that F/B = 1.03 (FSS) or 1.04 (RGM-H) for 100 MeV/c and F/B = 1.26 (FSS) or 1.33 (RGM-H) for 200 MeV/c. We compare in Fig. 10 the F/B ratios of FSS and RGM-H in the full calculation with the available experimental data [30,31] for the energy range up to $E_{\rm c.m.}$ = 20 MeV ($p_\Lambda \sim$ 310 MeV/c). Our prediction is within the upper limit of the experiment. We can conclude that the low-energy P wave Λp interaction is probably weakly attractive in accordance with the phenomenological analysis by Dalitz, Herndon, and Tang [32]. This weak attraction originates from the combined effect of the non-central force and the ΛN - $\Sigma N(I=1/2)$ coupling in our quark model.

Another spin observable related to the $LS^{(-)}$ force is the difference of the polarization of the scattered Λ (P_Λ) and the polarization of the recoil proton (P_N), which is shown in Fig. 8. This can be seen from the explicit expressions of these observables given in Table I of [22]. Since the invariant amplitudes, g and h in Eq.(2), vanish for the elastic scattering, we find $\sigma_0(\theta)\,P_{n000} = \Re e(a^*e + b^*f)$ and $\sigma_0(\theta)\,P_{0n00} = \Re e(a^*e - b^*f)$. The different signs of f indicate that one can tell the effect of the $LS^{(-)}$ force by observing the difference of $P_\Lambda = P_{n000}$ and $P_N = P_{0n00}$, since the amplitude f is related to the $LS^{(-)}$ force. Figure 8 shows apparent difference of P_Λ and P_N both in FSS and in RGM-H. These observables are measured experimentally as the left-right asymmetry of the differential cross sections when the out-going Λ or proton is rescattered in the target.

When the incident momentum of the Λ particle exceeds the ΣN threshold energy 638 MeV/c, the charge exchange reactions to $\Sigma^0 p$ and $\Sigma^+ n$ channels take place. The total reaction cross sections for $\Lambda p \to \Sigma^0 p$ are at most about $5 \sim 6$ mb for both of FSS and RGM-H, as is shown in Fig. 10(b) of [8]. If we use the isospin relation for the scattering amplitudes, the total reaction cross sections for $\Lambda p \to \Sigma^+ n$ are twice the above values. In

the next paper, we will discuss scattering observables for the $\Sigma^- p$ scattering, which also involves the charge exchange reactions to $\Sigma^0 n$ and Λn channels.

IV. SUMMARY

A study of the baryon-baryon interaction in the QCD-inspired quark model is motivated to clarify the rich low-energy hadron phenomena, which result from the non-perturbative quark dynamics dominated by an effective qq interaction and strong kinematical constraints of the quark Pauli principle and the symmetries of the spin, flavor, and color degrees of freedom. The most important findings of such studies are the importance of the quark degree of freedom in the short-range region and the very intricate roles of the meson-exchange effect in the medium- and long-range region. A realistic model for the baryon-baryon interaction with these facets of very different character should be examined by confronting the model predictions directly with the experimental data.

In this paper we have investigated scattering observables of the NN and YN interactions in the low- and intermediate-energy region by using a recent quark model developed for a simultaneous description of these interactions. Our model, called FSS [7,8] and RGM-H [8], and their preceding version RGM-F [15–17], is formulated in the $(3q)$-$(3q)$ resonating-group method (RGM), and incorporates a simple confinement potential of quadratic power law, the color analog of the full Fermi-Breit interaction with explicit quark-mass dependence, and minimum scalar (S) meson and pseudoscalar (PS) meson effective meson-exchange potentials directly coupled to quarks. RGM-F includes only π- and K-meson tensor force besides the central force of the full S-meson nonet, and the spin-flavor-color factors of the quark-exchange kernel is approximately evaluated. In the FSS and in most of the RGM-H, the spin-flavor-color factors of the quark exchange kernel are explicitly calculated for all the species of the S- and PS-meson nonets included. RGM-H is mainly different from FSS in using the same approximation as RGM-F exceptionally for the spin-flavor-color factors of the isoscalar S mesons. In FSS and RGM-H the model parameters are determined to fit the NN S-wave

and P-wave phase-shift values under the constraint of the deuteron binding energy and the $^1S_0$ scattering length, together with the low-energy YN "total" cross sections.

Before proceeding to the analysis of the YN scattering observables, we first examine the quality of our model by calculating the scattering observables of the np and pp systems, in which the rich knowledge of the phase shifts helps a great deal in understanding the characteristic features of the interaction pieces reflected in the scattering observables. The energy dependence and the angular-distribution shape of the differential cross sections, the polarization, and some other spin observables are qualitatively reproduced for the np and pp scattering in the wide energy region up to about 300 MeV, although our model slightly overestimates the differential cross sections on the high-energy side. In RGM-F, the lack of the spin-spin term of the PS-meson exchange potentials (the one-pion exchange, in particular) leads to some unsatisfactory behavior of the np differential cross sections and the spin correlation parameters at backward angles. Through this comparison, we can confirm that a particular component of the interaction pieces is strongly reflected in the characteristic behavior of some particular types of spin observables.

After making sure that the discrepancies between the predicted and empirical scattering observables in the NN system are far smaller than the ambiguity in the present experimental data for the YN interaction, we proceed to study scattering observables of the YN systems in FSS and RGM-H. When experimental data are not available, our predictions are compared with the corresponding values given by some OBEP models. It is found that the standard procedure to correlate the phase-shift behavior with the scattering observables is very useful even in the study of the YN interaction, in order to understand characteristic features of the model interactions appearing in the scattering observables.

In the study of Σ^+p scattering we have found large model-dependence in the predicted differential cross sections and the polarization at the intermediate energies $p_\Sigma = 400 \sim 800$ MeV/c. The behavior of some partial waves is strongly reflected in the energy dependence and the angular-distribution shape of the differential cross sections and the polarization. This includes the V-shape angular distribution of the differential cross sections in the

Nijmegen hard-core models [2,3] through the $^1P_1$ resonance around $p_\Sigma = 400$ MeV/c, and small differential cross sections in the Nijmegen soft-core model [4] and the Jülich models [5,6] through the $^3S_1$ resonance around $p_\Sigma = 400 \sim 600$ MeV/c. The differential cross sections predicted by FSS and RGM-H are very similar to each other, except that RGM-H overestimates the low-energy cross sections at $p_\Sigma \leq 200$ MeV/c. This similarity is related to the smooth energy dependence of the strongly repulsive $^3S_1$ phase shift and of the weakly attractive $^1P_1$ phase shift in our quark model. The differential cross sections at $p_\Sigma = 450$ MeV/c are compared to the recent KEK data [29] averaged over $p_\Sigma = 300 \sim 600$ MeV/c. Unfortunately, rather low statistics of this experimental data prevent us from obtaining new information on the Σ^+p interaction in the $^3S_1$ and $^1P_1$ states. As for the polarization in $p_\Sigma = 400 \sim 500$ MeV/c region, the Nijmegen model-F and the soft-core model gives relatively small values less than 0.1, while the Jülich models and our quark model yield appreciable values around 0.2.

In Λp system we have examined the scattering observables at the energy range below the ΣN threshold ($p_\Lambda = 638$ MeV/c). In this system the effect of non-central forces and the channel-coupling effect between ΛN and $\Sigma N(I = 1/2)$ configurations are both very important. The one-pion tensor force is responsible for the strong coupling among ΛN $^3S_1$, ΛN $^3D_1$, and $\Sigma N(I = 1/2)$ $^3S_1$ channels, yielding a prominent cusp structure for the Λp total cross sections at the ΣN threshold. Even below the ΣN threshold, this tensor coupling is important to make the ΛN $^3S_1$ phase shift very attractive. Among many models which reproduce low-energy Λp cross sections, our improved models FSS and RGM-H have characteristics that the $^1S_1$ state is very attractive and the $^3S_0$ state is less attractive. Besides a possible check of this feature in the energy spectra of s-shell Λ hypernuclei, we have found that the depolarization at low energies less than 200 MeV/c can be used to measure the difference of attraction between the $^1S_0$ and $^3S_1$ states. In the P-wave interaction, the effect of the $LS^{(-)}$ force is very important in our quark model. In particular, FSS gives a strong coupling between $^1P_1$ and $^3P_1$ channels by the $LS^{(-)}$ force generated from the Fermi-Breit interaction, resulting in strong enhancement of the cusp structure in the ΣN threshold

region. The effect of this coupling continues down to the energies of about 400 MeV/c. By examining the forward-to-backward ratio F/B of the differential cross sections, we find that the low-energy P-wave Λp interaction at $p_\Lambda \leq 300$ MeV/c is weakly attractive due to the combined effect of the LS and $LS^{(-)}$ forces, and of the ΛN - $\Sigma N(I = 1/2)$ channel coupling. As a direct detection of the the $LS^{(-)}$ force, we have pointed out that the scattered Λ-particle and the recoil proton have almost opposite signs in the polarization at intermediate energies. The Wolfenstein parameters at $p_\Lambda = 600$ MeV/c are also calculated in FSS and RGM-H. Because of the quantitative difference in the strength of the ΛN - $\Sigma N(I = 1/2)$ coupling, they give a sizable difference comparable to the difference from the other OBEP models. This indicates that more experimental information is indispensable, in order to understand the whole picture of the Λp interaction.

In summary, we have found that various YN interaction models, which reproduce the NN and YN experimental data currently available, sometimes give entirely different predictions for the YN scattering observables in the intermediate-energy region, where experimental data are not yet available. This indicates that many of the models have quite different characteristics from each other, with respect to the relative importance of the different partial waves, the relative strength of the central and non-central forces, the cancellation mechanism of the short-range repulsion and the intermediate-range attraction and so on. The behavior of the phase shifts for the P wave and the higher partial waves cannot be determined only from the low-energy YN cross section data currently available. Once new data are obtained in the intermediate-energy region, the scattering observables could give important information that makes it possible to construct better models for the realistic description of the various YN interactions.

ACKNOWLEDGMENTS

The authors would like to thank members of the Nuclear Theory Group of Kyoto University for useful discussions. This work was supported by the Grants-in-Aid for Scientific Research from the Ministry of Education, Science and Culture (07640397, 08239203, and 09225201).

REFERENCES

[1] M. Oka, and K. Yazaki, in *Quarks and Nuclei*, ed. W. Weise (World Scientific, Singapore, 1984), p. 489; K. Shimizu, Rep. Prog. Phys. **52**, 1 (1989); C. W. Wong, Phys. Rep. **136**, 1 (1986).

[2] M. M. Nagels, T. A. Rijken, and J. J. de Swart, Phys. Rev. **D15**, 2547 (1977).

[3] M. M. Nagels, T. A. Rijken, and J. J. de Swart, Phys. Rev. **D20**, 1633 (1979).

[4] P. M. M. Maessen, Th. A. Rijken, and J. J. de Swart, Phys. Rev. **C40**, 2226 (1989).

[5] B. Holzenkamp, K. Holinde, and J. Speth. Nucl. Phys. **A500**, 485 (1989).

[6] A. Reuber, K. Holinde, and J. Speth, Nucl. Phys. **A570**, 543 (1994).

[7] Y. Fujiwara, C. Nakamoto, and Y. Suzuki, Phys. Rev. Lett. **76**, 2242 (1996).

[8] Y. Fujiwara, C. Nakamoto, and Y. Suzuki, Phys. Rev. **C54**, 2180 (1996).

[9] T. Fujita, Y. Fujiwara, C. Nakamoto, Y. Suzuki, T. Yamamoto, and R. Tamagaki, Prog. Theor. Phys. **96**, 463 (1996).

[10] T. Fujita, Y. Fujiwara, C. Nakamoto, and Y. Suzuki, Prog. Theor. Phys. **96**, 653 (1996).

[11] R. Vinh Mau, C. Semay, B. Loiseau, and M. Lacombe, Phys. Rev. Lett. **67**, 1392 (1991).

[12] S. Takeuchi, K. Shimizu, and K. Yazaki, Nucl. Phys. **A504**, 777 (1989).

[13] A. I. Machavariani, U. Straub, and Amand Faessler, Nucl. Phys. **A548**, 592 (1992).

[14] D. R. Entem, A. I. Machavariani, A. Valcarce, A. J. Buchmann, Amand Faessler, and F. Fernández, Nucl. Phys. **A602**, 308 (1996).

[15] C. Nakamoto, Y. Suzuki, and Y. Fujiwara, Prog. Theor. Phys. **94**, 65 (1995).

[16] Y. Fujiwara, C. Nakamoto, and Y. Suzuki, Prog. Theor. Phys. **94**, 215 (1995).

[17] Y. Fujiwara, C. Nakamoto, and Y. Suzuki, Prog. Theor. Phys. **94**, 353 (1995).

[18] V. G. J. Stoks, R. A. M. Klomp, M. C. M. Rentmeester, and J. J. de Swart, Phys. Rev. **C48**, 792 (1993).

[19] V. G. J. Stoks, R. A. M. Klomp, C. P. F. Terheggen, and J. J. de Swart, Phys. Rev. **C49**, 2950 (1994).

[20] Fl. Stancu, S. Pepin, and L. Ya. Glozman, Phys. Rev. **C56**, 2779 (1997).

[21] M. Kamimura, Prog. Theor. Phys. Suppl. **62**, 236 (1977).

[22] J. Bystricky, F. Lehar, and P. Winternitz, J. de Phys. **45**, 207 (1984).

[23] J. Bystricky, C. Lechanoine-Leluc, and F. Lehar, J. de Phys. **48**, 199 (1987).

[24] Y. Fujiwara, C. Nakamoto, Y. Suzuki, and Zhang Zong-ye, Prog. Theor. Phys. **97**, 587 (1997).

[25] J. Bystricky, F. Lehar, and P. Winternitz, J. de Phys. **39**, 1 (1978).

[26] H. P. Stapp, Phys. Rev. **103**, 425 (1956).

[27] N. Hoshizaki, Prog. Theor. Phys. Suppl. **42**, 107 (1968).

[28] Scattering Analysis Interactive Dial-up (SAID), Virginia Polytechnic Institute, Blacksburg, Virginia (R. A. Arndt, private communication).

[29] Y. Goto, Memoirs of the Faculty of Science, Kyoto University, Series A of Physics, Astrophysics, Geophysics and Chemistry, Vol. XXXX, No. 1, 1 (1997).

[30] G. Alexander, U. Karshon, A. Shapira, G. Yekutieli, R. Engelmann, H. Filthuth, and W. Lughofer, Phys. Rev. **173**, 1452 (1968).

[31] B. Sechi-Zorn, B. Kehoe, J. Twitty, and R. A. Burnstein, Phys. Rev. **175**, 1735 (1968).

[32] R. H. Dalitz, R. C. Herndon, and Y. C. Tang, Nucl. Phys. **B47**, 109 (1972).

[33] Th. A. Rijken, P. M. M. Maessen, and J. J. de Swart, Nucl. Phys. **A547**, 245c (1992).

TABLES

TABLE I. Quark-model parameters, SU_3 parameters of the EMEP, S-meson masses, and the reduction factor c_δ for FSS and RGM-H. The parameter α denotes the $F/(F+D)$ ratio for the flavor-octet SU_3 coupling constants. The ϵ-meson mass denoted by "two-pole" indicates two-pole approximation, for which m_1c^2 (β_1) and m_2c^2 (β_2) are shown below the table.

	b (fm)	$m_{ud}c^2$ (MeV)	α_S	$\lambda = m_s/m_{ud}$
FSS	0.616	360	2.1742	1.526
RGM-H	0.667	389	2.1680	1.490
	f_1^S	f_8^S	θ_S (deg)	α
FSS	2.89138	1.07509	27.78[a]	1
RGM-H	2.95388	0.86906	36.018	1.32[b]
	f_1^{PS}	f_8^{PS}	θ_{PS} (deg)	α
FSS	0.21426	0.26994	−23	2/5
RGM-H	0.15853	0.26410	−23	2/5
	$m_\epsilon c^2$ (MeV)	$m_{S^*}c^2$ (MeV)	$m_\delta c^2$ (MeV)	$m_\kappa c^2$ (MeV)
FSS	800	1250	970	1145
RGM-H	two-pole[c]	1250	980	920
	c_δ			
FSS	0.381			
RGM-H	0.339			

[a] $\theta_S = 65°$ is used in the $\Sigma N(I=3/2)$ channel.

[b] $\alpha = 1$ for non-isoscalar mesons.

[c] 487.818 MeV (0.16900) and 1021.14 MeV (0.61302) [19].

TABLE II. Λp $^1S_0$ and $^3S_1$ phase shifts at $p_\Lambda = 200$ MeV/c and effective range parameters predicted by our quark model, RGM-F, FSS and RGM-H. The corresponding values by some OBEP's, Nijmegen hard-core model-D (HC-D) [2], hard-core model-F (HC-F) [3], and soft-core model (NSC) [4], are also shown for comparison.

	HC-D	HC-F	NSC	RGM-F	FSS	RGM-H
$^1S_0$	24°	29°	33°	29°	46°	45°
$^3S_1$	28°	27°	25°	33°	17°	17°
a_s (fm)	−1.90	−2.29	−2.78	−2.03	−5.39	−5.34
r_s (fm)	3.72	3.17	2.88	3.05	2.26	2.46
a_t (fm)	−1.96	−1.88	−1.41	−2.48	−1.02	−1.04
r_t (fm)	3.24	3.36	3.11	2.69	4.21	4.91

TABLE III. Λp P-wave phase shifts (in degrees) predicted by FSS and RGM-H at energies below the ΣN threshold. $^3P_0$, $^3P_2$, $^1P_1$, $^3P_1$ phase shifts and the mixing angle ρ_1 for $^1P_1$-$^3P_1$ coupling are listed.

p_Λ	$^3P_0$		$^3P_2$		$^1P_1$		$^3P_1$		ρ_1	
(MeV/c)	FSS	RGM-H	FSS	RGM-H	FSS	RGM-H	FSS	RGM-H	FSS	RGM-H
100	−0.01	0.04	0.15	0.22	0.05	0.05	0.05	0.07	−0.11	−0.07
200	−0.12	0.14	1.12	1.57	0.46	0.34	0.38	0.42	−0.85	−0.54
300	−0.64	−0.12	3.29	4.37	1.90	0.98	1.30	0.92	−2.94	−1.70
400	−1.94	−1.33	6.41	7.91	5.58	2.01	3.36	1.22	−7.35	−3.69
500	−4.21	−3.73	9.70	11.15	14.22	3.70	7.79	1.28	−15.93	−6.65
600	−7.28	−7.08	12.45	13.53	36.90	7.21	14.21	2.20	−32.44	−11.46

FIGURES

FIG. 1. Comparison of the quark-model np differential cross sections and polarization with experimental data. The solid curve denotes the result by RGM-H, and the dashed curve by FSS. The model calculation takes into account the partial waves up to $J_{\max} = 7$. The experimental data are taken from [28].

FIG. 2. The same as Fig. 1 but for pp differential cross sections and polarization.

FIG. 3. Depolarization D and Wolfenstein parameters R and A by RGM-H (solid curve) and FSS (dashed curve) for np system, compared with experimental data [28].

FIG. 4. The same as Fig. 3 but for pp depolarization and Wolfenstein parameters R at various energies.

FIG. 5. The same as Fig. 4 but for pp Wolfenstein parameters R' and A.

FIG. 6. Quark-model predictions for $\Sigma^+ p$ differential cross sections and polarization in RGM-H (solid curve) and FSS (dashed curve), compared with those by the Nijmegen soft-core model, NSC (circles), and the hard-core model-F, HC-F (crosses). The results by NSC and HC-F are obtained by using the phase-shift values given in [4] and [3] with the maximum angular-momentum values up to $l \leq 2$ and $l \leq 4$, respectively. For FSS and RGM-H, partial waves up to $J_{\max} = 7$ are included.

FIG. 7. The differential cross sections and the depolarization for Λp system predicted by RGM-H (solid curve) and FSS (dashed curve). The partial waves up to $J_{\max} = 7$ are taken into account. Predictions by NSC (circles) and Jülich B (diamonds), which are taken from [33] and [6], respectively, are also shown for $p_\Lambda = 600$ MeV/c.

FIG. 8. The same as Fig. 7, but for the polarization of the scattered (P_Λ) and recoil (P_N) particles.

FIG. 9. Wolfenstein parameters, R, R', A, and A', at $p_\Lambda = 600$ MeV/c. The quark-model calculation by RGM-H (solid curve) and FSS (dashed curve) includes contributions from the partial waves up to $J_{\max} = 7$. The predictions by NSC (circles) and Jülich B (diamonds) are taken from [33] and [6], respectively.

FIG. 10. Forward-to-backward ratio of Λp differential cross sections by RGM-H (solid curve) and FSS (dashed curve), compared with the experimental data [30,31].

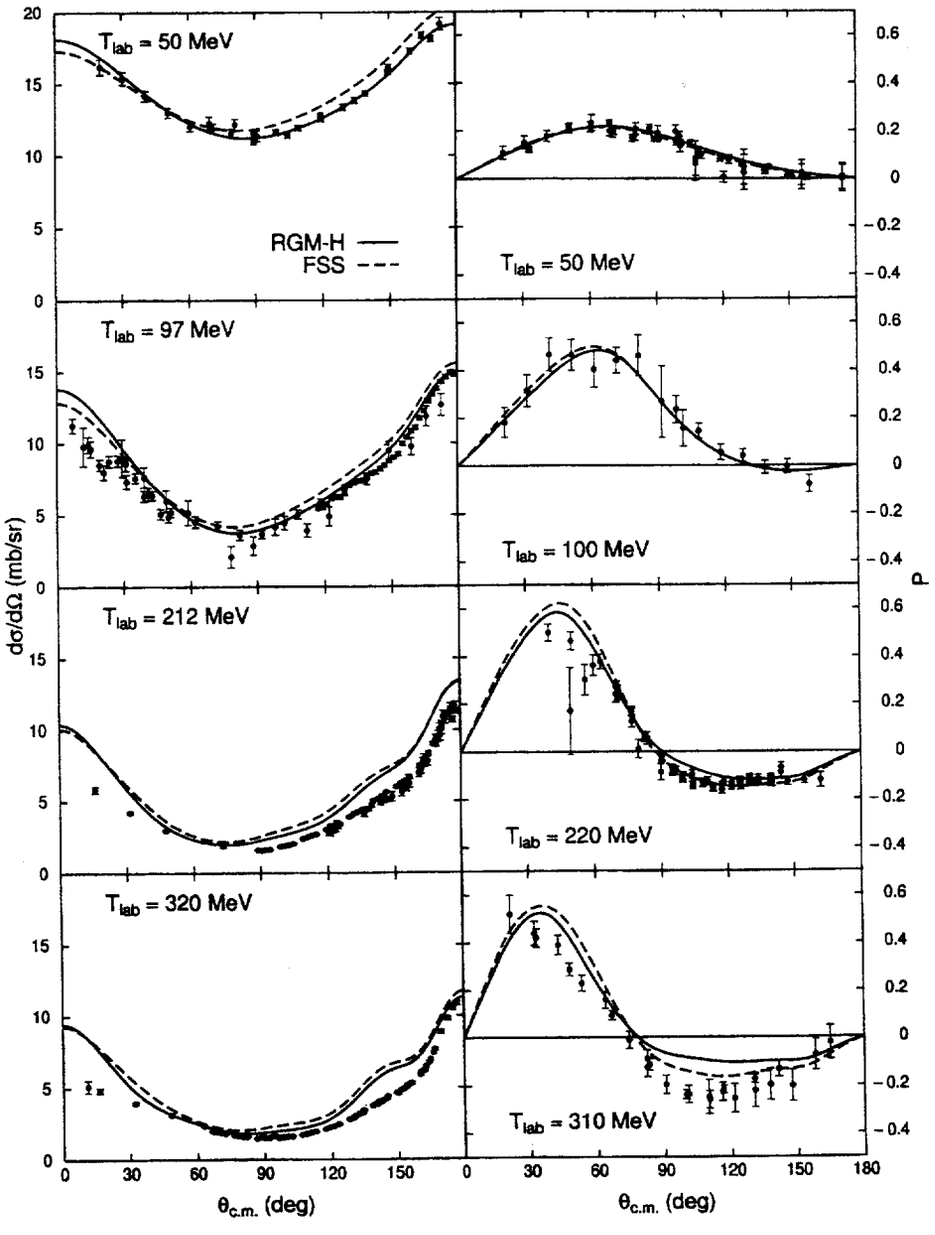
T_lab = 50 MeV
RGM-H
FSS
T_lab = 50 MeV
T_lab = 97 MeV
T_lab = 100 MeV
T_lab = 212 MeV
T_lab = 220 MeV
T_lab = 320 MeV
T_lab = 310 MeV
dσ/dΩ (mb/sr)
P
θc.m. (deg)
θc.m. (deg)

FIG. 1

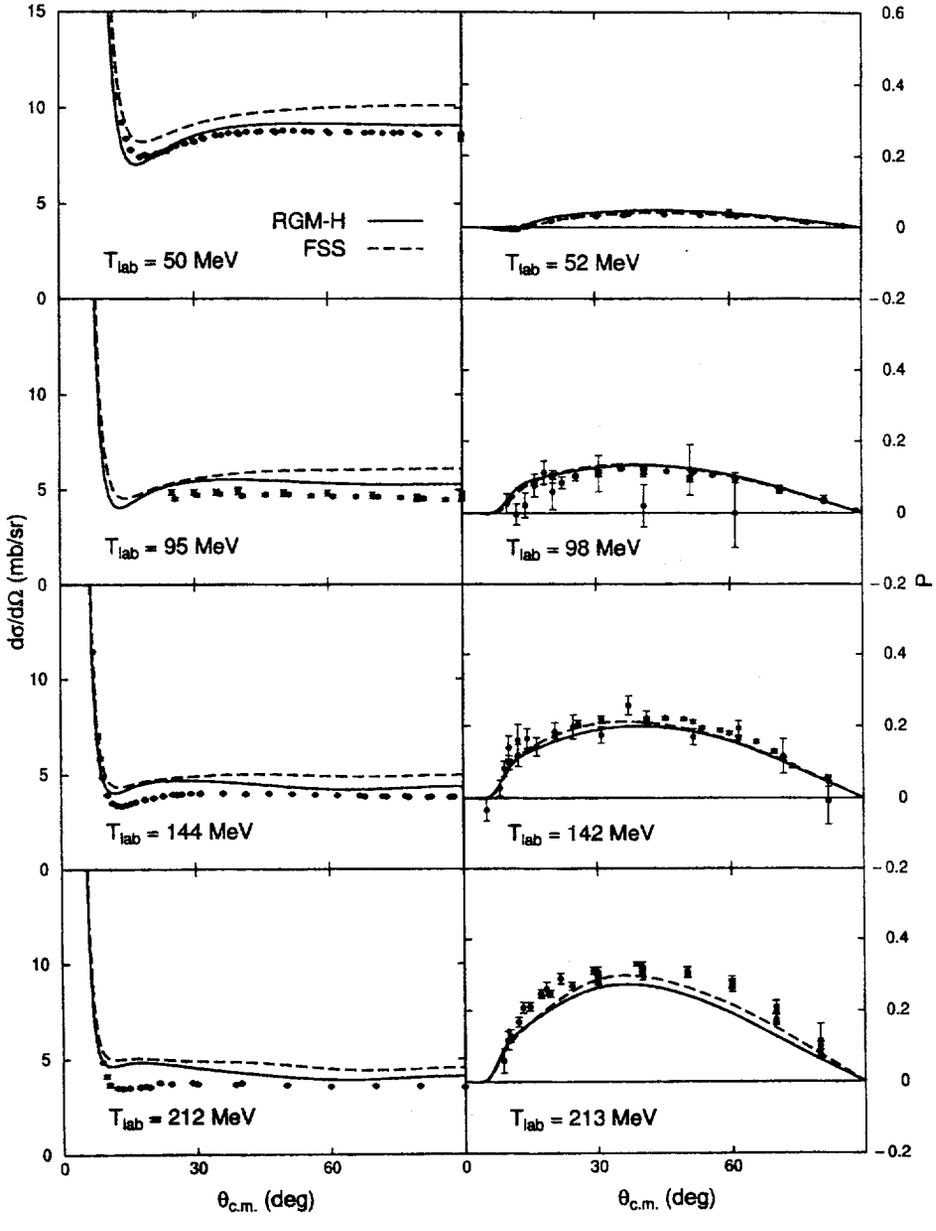
RGM-H
FSS
T_lab = 50 MeV
T_lab = 52 MeV
T_lab = 95 MeV
T_lab = 98 MeV
T_lab = 144 MeV
T_lab = 142 MeV
T_lab = 212 MeV
T_lab = 213 MeV
dσ/dΩ (mb/sr)
P
θc.m. (deg)
θc.m. (deg)

FIG. 2

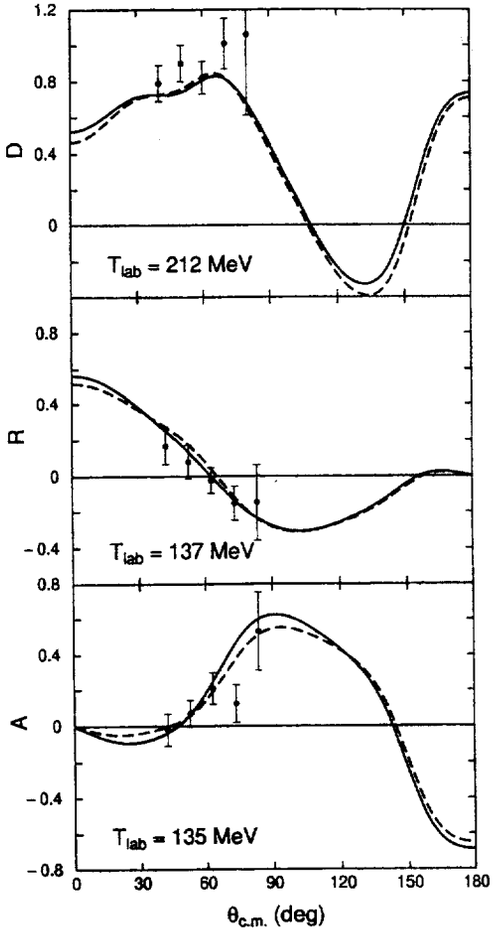
D
R
A
T_{lab} = 212 MeV
T_{lab} = 137 MeV
T_{lab} = 135 MeV
$\theta_{c.m.}$ (deg)

FIG. 3

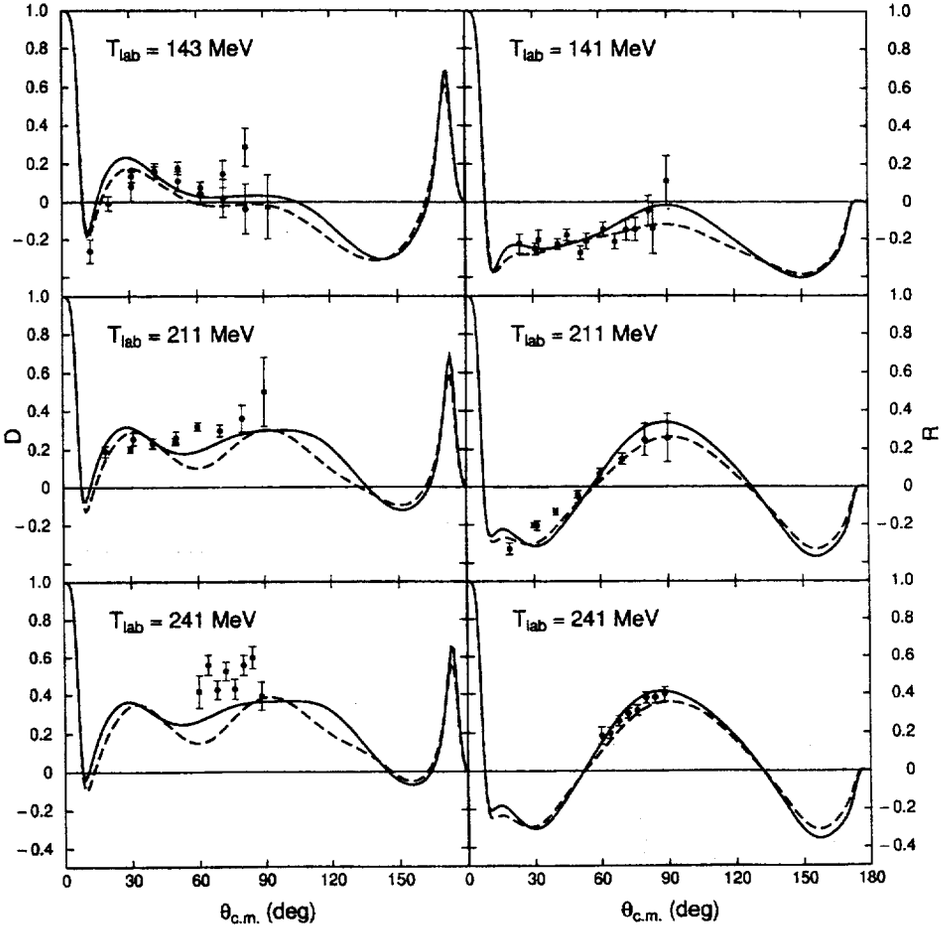
D
R
T_{lab} = 143 MeV
T_{lab} = 141 MeV
T_{lab} = 211 MeV
T_{lab} = 211 MeV
T_{lab} = 241 MeV
T_{lab} = 241 MeV
$\theta_{c.m.}$ (deg)
$\theta_{c.m.}$ (deg)

FIG. 4

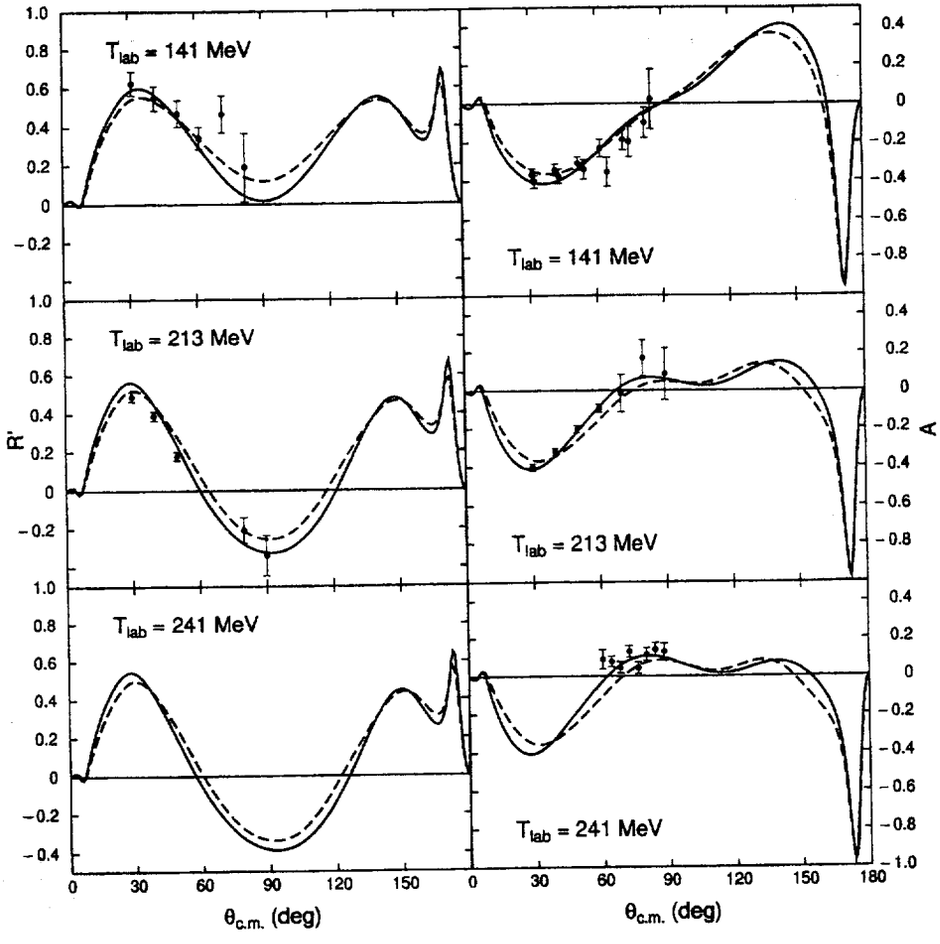
T_{lab} = 141 MeV
T_{lab} = 213 MeV
T_{lab} = 241 MeV
R'
A
$\theta_{c.m.}$ (deg)

FIG. 5

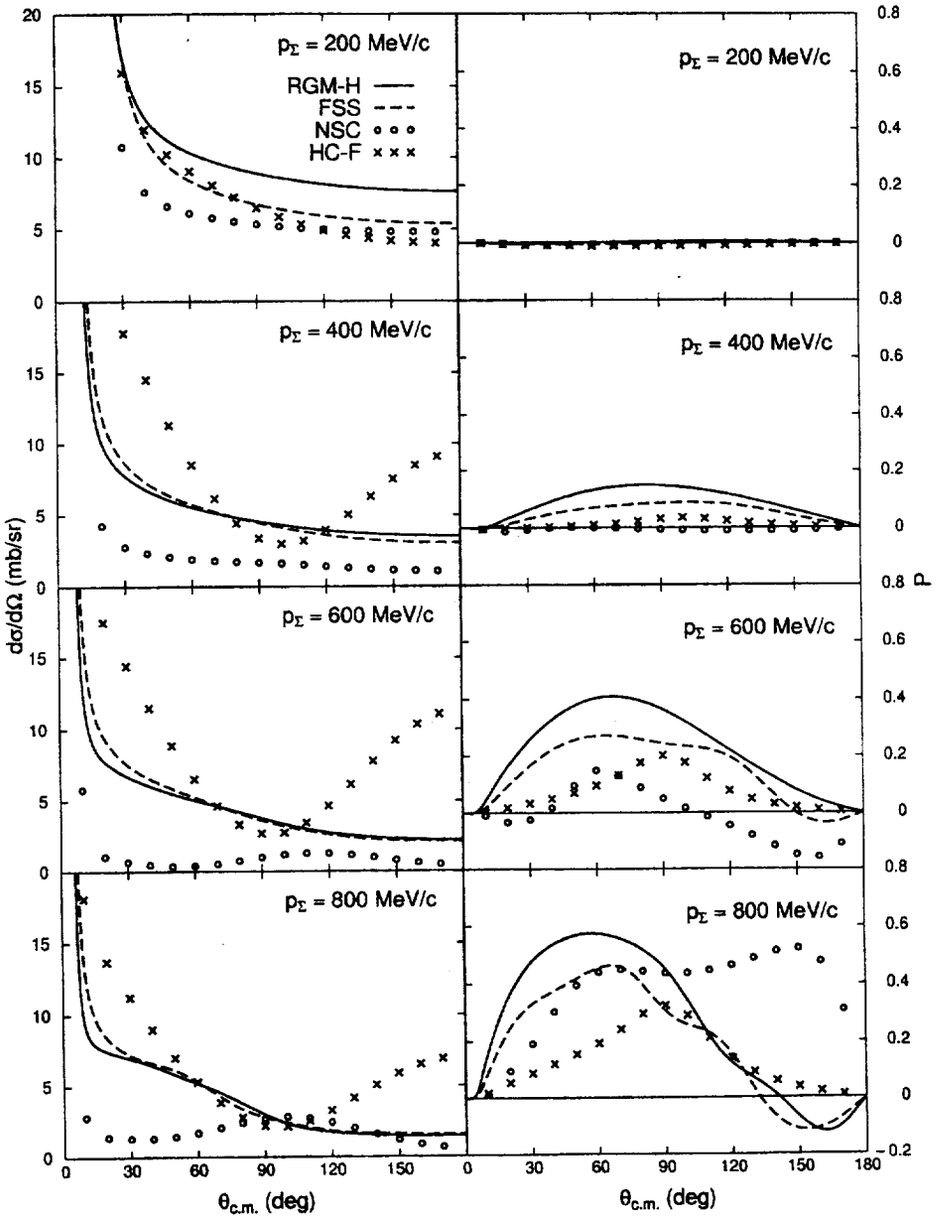
p_Σ = 200 MeV/c
RGM-H
FSS
NSC
HC-F
p_Σ = 400 MeV/c
p_Σ = 600 MeV/c
p_Σ = 800 MeV/c
$d\sigma/d\Omega$ (mb/sr)
P
$\theta_{c.m.}$ (deg)

FIG. 6

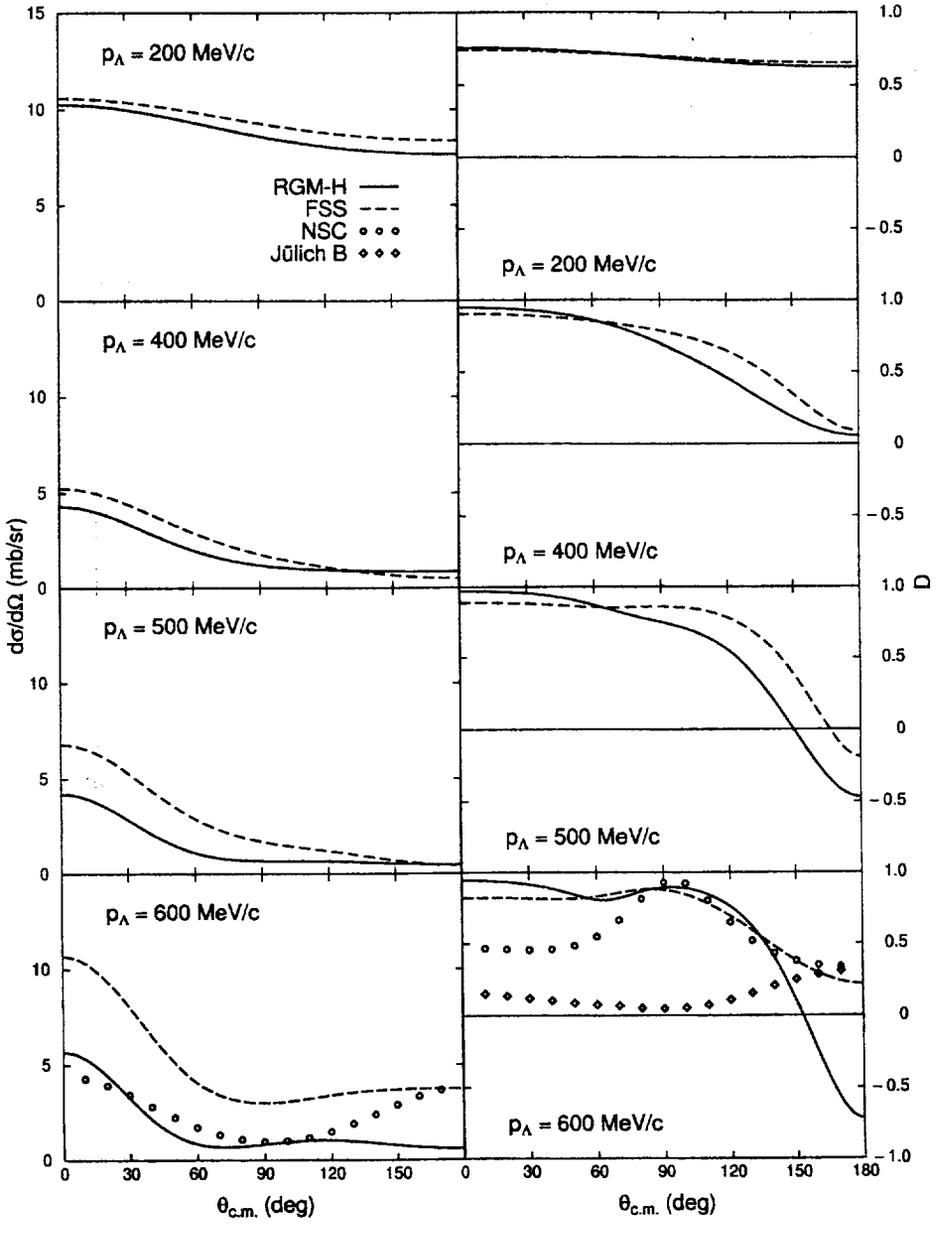
p_Λ = 200 MeV/c
RGM-H
FSS
NSC
Jülich B
p_Λ = 400 MeV/c
p_Λ = 500 MeV/c
p_Λ = 600 MeV/c
dσ/dΩ (mb/sr)
D
$\theta_{c.m.}$ (deg)

FIG. 7

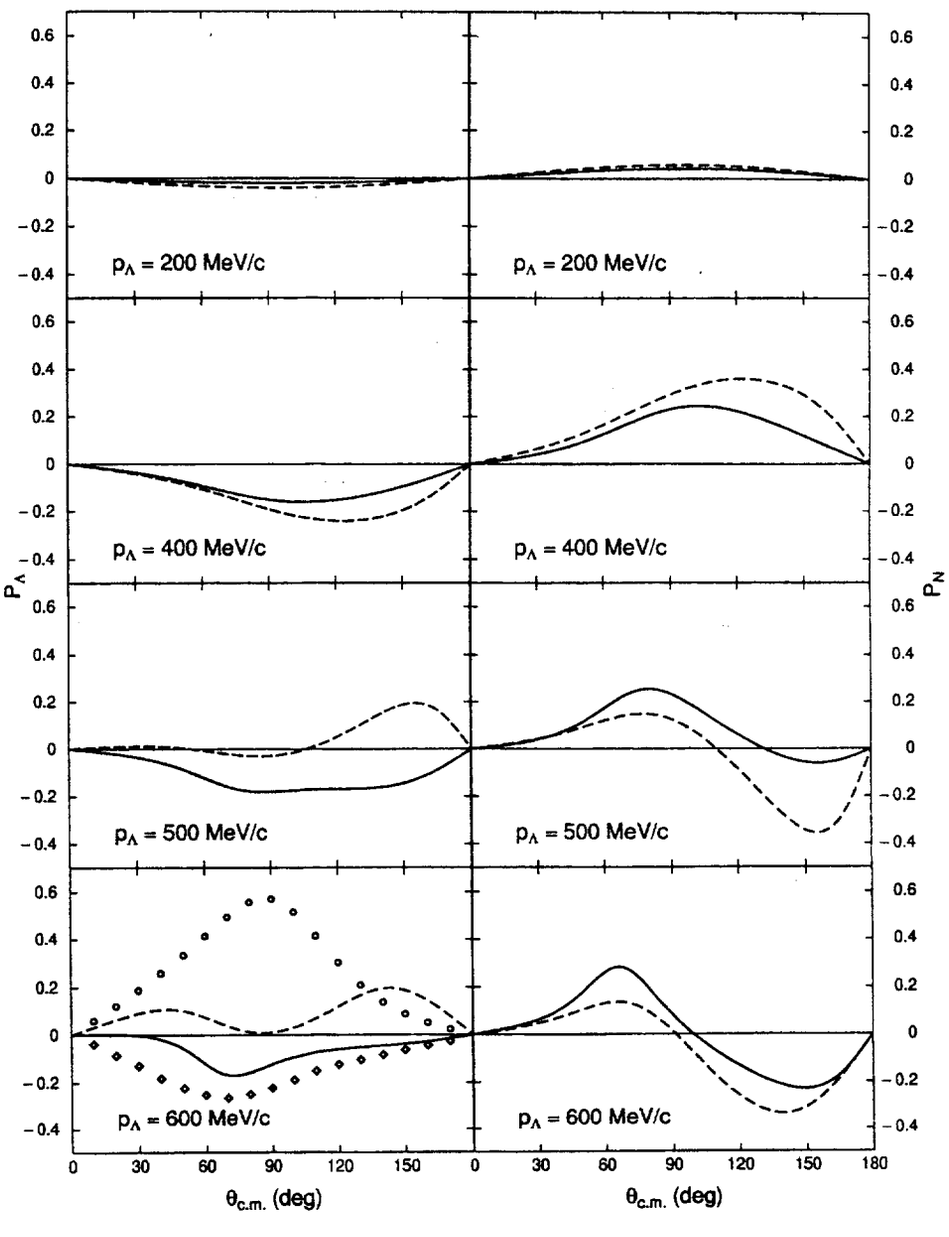
p_Λ = 200 MeV/c
p_Λ = 400 MeV/c
p_Λ = 500 MeV/c
p_Λ = 600 MeV/c
P_Λ
P_N
$\theta_{c.m.}$ (deg)

FIG. 8

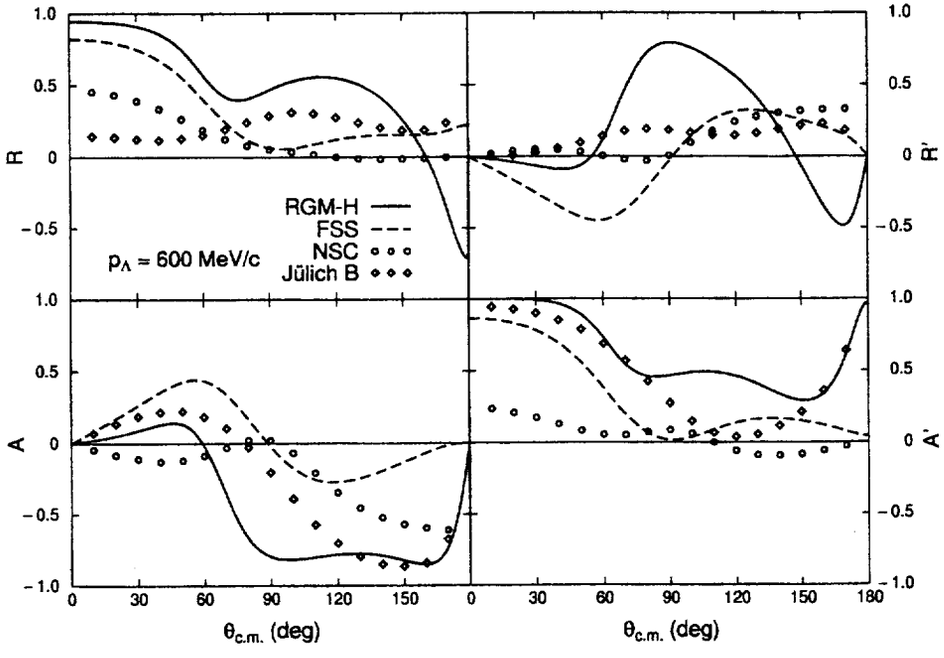
R
A
R̃
Ã
RGM-H
FSS
NSC
Jülich B
p_Λ = 600 MeV/c
$\theta_{c.m.}$ (deg)
$\theta_{c.m.}$ (deg)

FIG. 9

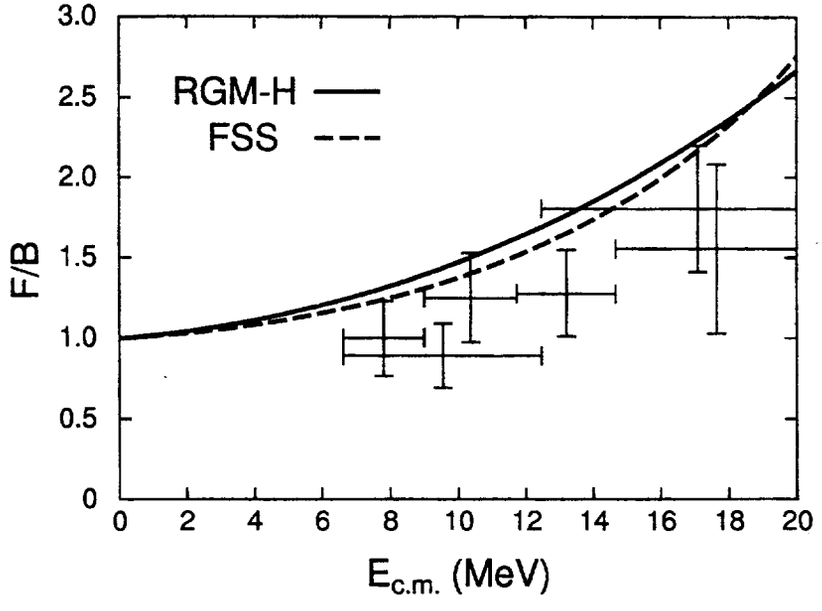
F/B
RGM-H
FSS
$E_{c.m.}$ (MeV)

FIG. 10